Earth's Future

RESEARCH ARTICLE
10.1029/2021EF002462

Correlation Between Sea-Level Rise and Aspects of Future Tropical Cyclone Activity in CMIP6 Models

Joseph W. Lockwood[1], Michael Oppenheimer[1,2,3], Ning Lin[4], Robert E. Kopp[5,6], Gabriel A. Vecchi[1,3,7], and Avantika Gori[4]

[1]Department of Geoscience, Princeton University, Princeton, NJ, USA, [2]Princeton School of Public and International Affairs, Princeton University, Princeton, NJ, USA, [3]High Meadows Environmental Institute, Princeton, NJ, USA, [4]Civil and Environmental Engineering, Princeton University, Princeton, NJ, USA, [5]Institute of Earth, Ocean, and Atmospheric Sciences, Rutgers University, New Brunswick, NJ, USA, [6]Department of Earth and Planetary Sciences, Rutgers University, Piscataway, NJ, USA, [7]Atmospheric and Oceanic Sciences Program, Princeton University, Princeton, NJ, USA

Key Points:

- Relative sea-level rise (SLR) at many locations is strongly correlated with vertical wind shear (negatively) and potential intensity (positively)
- Global mean surface air temperature change is found to modulate the co-variability between SLR and tropical cyclone activity
- Flood hazard assessments that neglect the joint influence of these factors may not accurately represent future flood hazard

Supporting Information:

Supporting Information may be found in the online version of this article.

Correspondence to:

J. W. Lockwood,
jl115@princeton.edu

Citation:

Lockwood, J. W., Oppenheimer, M., Lin, N., Kopp, R. E., Vecchi, G. A., & Gori, A. (2022). Correlation between sea-level rise and aspects of future tropical cyclone activity in CMIP6 models. *Earth's Future*, *10*, e2021EF002462. https://doi.org/10.1029/2021EF002462

Received 29 SEP 2021
Accepted 20 MAR 2022

Abstract Future coastal flood hazard at many locations will be impacted by both tropical cyclone (TC) change and relative sea-level rise (SLR). Despite sea level and TC activity being influenced by common thermodynamic and dynamic climate variables, their future changes are generally considered independently. Here, we investigate correlations between SLR and TC change derived from simulations of 26 Coupled Model Intercomparison Project Phase 6 models. We first explore correlations between SLR and TC activity by inference from two large-scale factors known to modulate TC activity: potential intensity (PI) and vertical wind shear. Under the high emissions SSP5-8.5, SLR is strongly correlated with PI change (positively) and vertical wind shear change (negatively) over much of the western North Atlantic and North West Pacific, with global mean surface air temperature (GSAT) modulating the co-variability. To explore the impact of the joint changes on flood hazard, we conduct climatological–hydrodynamic modeling at five sites along the US East and Gulf Coasts. Positive correlations between SLR and TC change alter flood hazard projections, particularly at Wilmington, Charleston and New Orleans. For example, if positive correlations between SLR and TC changes are ignored in estimating flood hazard at Wilmington, the average projected change to the historical 100 years storm tide event is under-estimated by 12%. Our results suggest that flood hazard assessments that neglect the joint influence of these factors and that do not reflect the full distribution of GSAT change may not accurately represent future flood hazard.

Plain Language Summary Future coastal flood hazard at many locations will be influenced by sea level rise (SLR) and tropical cyclone (TC) activity. Due to their common dependence on the wider climate system, TC activity and SLR may increase in a joint manner with progressive warming. To explore joint variability, we first analyze correlations between SLR and future TC activity by inference from two large-scale climate factors known to modulate TC activity. SLR is strongly correlated with the two large-scale climate factors over much of the western North Atlantic and North West Pacific, with global mean surface air temperature (GSAT) modulating the joint changes. Using a set of synthetic TC events and a storm tide model, we find that positive correlations between SLR and TC change alter flood hazard projections, particularly at Wilmington, Charleston and New Orleans. Our results suggest that flood hazard assessments that neglect the joint influence of these factors and that do not reflect the full distribution of GSAT change may not accurately capture future flood hazard.

1. Introduction

Coastal flooding in the context of future tropical cyclone (TC) variability, sea-level rise (SLR) and shoreline change is one of the most important issues facing coastal populations (Woodruff et al., 2013). Climate change is increasing the threat posed by TCs to coastal regions (Camargo & Wing, 2021; Knutson et al., 2020; Reed et al., 2015; Wang & Toumi, 2021), with flood events driven by TC storm surges expected to increase into the future as a result of accelerated SLR elevating the baseline on which these events occur (Bilskie et al., 2014, 2016; De Dominicis et al., 2020; Garner et al., 2017; Idier et al., 2019; Kirezci et al., 2020; Lin et al., 2012; Liu et al., 2019; Marsooli et al., 2019; Marsooli & Lin, 2020; Reed et al., 2015; Vousdoukas et al., 2018; Woodruff et al., 2013). Historical SLR, for example, is estimated to have added $8.1 billion ($4.7–$14.0, 5th–95th percentiles) to cost of damages caused by Hurricane Sandy's (2012) storm surge (Strauss et al., 2021). At many locations, future

flood hazard may also be compounded by changes in TC climatology (Lin et al., 2012, 2016; Little et al., 2015; Marsooli et al., 2019; Marsooli & Lin, 2020; Reed et al., 2015). The potential compound effect of sea level change and TC activity is best exemplified by supertyphoon Haiyan (2013). Observed increases in regional sea surface temperatures and ocean heat content since 1993, likely contributed to both the typhoon's extreme wind speeds and regional SLR. This regional SLR meant that Haiyan's extreme storm surge was on a baseline sea level some 30 cm above levels in 1993 (Trenberth et al., 2015).

Superimposed on the global SLR, which is driven by ocean thermal expansion and by melting land ice loss, relative sea levels may change owing to vertical land movement (VLM) and dynamic sea level changes. The sterodynamic component of relative SLR, composed of ocean thermal expansion and regional ocean steric and dynamic effects (Gregory et al., 2019), is derived from atmosphere–ocean general circulation models (AOGCMs) that do not simulate SLR contributions from melting land ice and local non-climatic SLR associated with VLM and glacial isostatic adjustment (GIA) (Gregory et al., 2019; Griffies et al., 2016; Kopp et al., 2014, 2015). Estimates of land ice contributions to SLR are instead derived from physical models of varying degree of complexity (Levermann et al., 2020; Oppenheimer et al., 2019) or from results of structured expert elicitation (Bamber et al., 2019). In probabilistic analyses, variance in global mean sea level rise (GMSLR) and local SLR at many locations in the early 21st century relates predominately to sterodynamic SLR, due to large AOGCM spread in projected changes (Kopp et al., 2014, 2017). In the global average and at many locations, the Antarctic ice-sheet is the dominant source of variance in late 21st century SLR projections (Kopp et al., 2014, 2017).

Climate change is also expected to alter aspects of TC activity into the future. As reviewed by Knutson et al. (2020), there is moderately strong consensus on a model-projected increase in high intensity TCs, in TCs rainfall and in an increase in storm-surge flooding due to SLR, assuming all other factors are unchanged. Considerable uncertainty remains in the projection of future TCs, particularly regarding changes in frequency, translation speed and average latitude at which TCs reach their lifetime-maximum intensity (Knutson et al., 2020), and their dependence on the large-scale climate. Low-resolution AOGCMs, which are often used to investigate TCs, generally cannot resolve category 3–5 TCs or poorly simulate the frequency and spatial distribution of category 3–5 TCs compared to observations (Knutson et al., 2020; Vecchi et al., 2019; Yin et al., 2020). These low resolution AOGCMs generally project decreases in global TC frequency under climate change (Knutson et al., 2020). In contrast, some studies project no change (Camargo, 2013; Vecchi et al., 2019) or increases in global TC frequency (Bhatia et al., 2018; Emanuel, 2013, 2021; Vecchi et al., 2019).

Due to their common dependence on large-scale climate variables, SLR and TC activity change are expected to co-vary into the future (Little et al., 2015). Joint variability will be driven in part by atmospheric warming, which will increase SLR through ocean heat uptake and thermal expansion, and by melting land ice (Church et al., 2013; Fox-Kemper et al., 2021; Oppenheimer et al., 2019) as well as the theoretical maximum wind speed (PI) of TCs in some regions (Emanuel, 2013; Sobel et al., 2016; Vecchi & Soden, 2007a, 2007c). Concurrent changes in sea level and TC activity may also be driven by changes in fluxes of momentum and heat at the ocean surface that impact both dynamic sea level (Yin et al., 2020) and TC circulation and intensification (Emanuel, 2004).

At present, there is limited analysis of the joint variability between relative SLR and TC activity change, and its implications for coastal flood hazard. Little et al. (2015) project changes in surge hazard focusing on sterodynamic SLR and power dissipation index (PDI; an integrated measure of TC intensity, frequency and duration) changes at 5 sites along the US East Coast—the latter derived from a 15-member ensemble of climate models following a statistical modeling approach (Villarini & Vecchi, 2013). Sterodynamic SLR and PDI projections along the US East Coast are found to co-vary, with joint increases compounding projected flood hazard (Little et al., 2015). However, the projected increases in Atlantic PDI have considerable uncertainty; for example, several other TC modeling studies using dynamical, rather than statistical, downscaling approaches project no change or reductions in PDI (Knutson et al., 2015; Yamada et al., 2010).

Recent research shows that joint variability and dependence structures between climate variables often strongly affect the occurrence frequency and intensity of multivariate extremes (Little et al., 2015; Wahl et al., 2015; Zscheischler et al., 2018; Zscheischler & Seneviratne, 2017). However, flood hazard assessments assume that SLR and TC characteristics are independent, conditional on the emissions pathway (Garner et al., 2017; Idier et al., 2019; Lin et al., 2012; Marsooli et al., 2019; Marsooli & Lin, 2020). Assessments that explore projected changes in TCs generally either combine storm surges with a limited number of SLR scenarios (Bilskie et al., 2014, 2016;

Idier et al., 2019; Lin et al., 2012; Liu et al., 2019) or with probabilistic SLR projections that are derived in part from a subset of AOGCMs (Garner et al., 2017; Lin et al., 2016; Marsooli et al., 2019; Marsooli & Lin, 2020; Vousdoukas et al., 2018). On the other hand, assessments that evaluate changes in flood hazard due to SLR usually assume that the statistical nature of TC storm surges will remain unchanged (Buchanan et al., 2016; Frederikse et al., 2020; Hunter, 2011; Kirezci et al., 2020; Kopp et al., 2014, 2017; Rasmussen et al., 2018; Tebaldi et al., 2012). By neglecting joint changes in TC activity and SLR (Buchanan et al., 2016; Frederikse et al., 2020; Hunter, 2011; Kirezci et al., 2020; Kopp et al., 2014, 2017; Rasmussen et al., 2018; Tebaldi et al., 2012) or by assuming independence (Garner et al., 2017; Idier et al., 2019; Lin et al., 2012; Marsooli et al., 2019; Marsooli & Lin, 2020), assessments may fail to fully represent future flood hazard.

Although there is strong confidence in accelerated SLR intensifying TC storm surge into the future, only a limited number of studies have assessed the role of joint changes in TC activity and sea level to future multivariate extreme events. This paper aims to address this gap by answering the follow questions: (a) Are relative SLR and large-scale factors known to modulate TC activity (PI and vertical wind shear) correlated within the wider climate system, and what are the time scales and emissions scenarios over which these correlations apply? (b) Do the broad-scale joint changes translate into meaningful differences in flood hazards at a local scale? To answer these questions, we first investigate correlations between relative SLR and two large-scale factors (PI and vertical wind shear) known to modulate TC activity derived from simulations of 26 Coupled Model Intercomparison Project Phase 6 (CMIP6) models, across a range of emissions scenarios. We next conduct climatology–hydrodynamic modeling for eight CMIP6 models under SSP5-8.5 to quantify the impact of joint changes to future coastal flood events at five sites (New York City NY, Wilmington NC, Charleston SC, Miami FL and New Orleans LA) along the US East and Gulf Coast, focusing primarily on Wilmington, NC.

2. Methods

We assess correlations and co-variability between SLR and TC change using models from the CMIP6 (Eyring et al., 2016). CMIP6 models comprise a range of AOGCMs and Earth System Models (ESMs), differing from each other in terms of model structure, including vertical coordinate, grid resolution and sub-grid parameterizations. We limit our analysis to models that have the variables necessary to compute PI, dynamic sea-level change and vertical wind shear. We use only a single run ("r1i1p1") for each CMIP6 model. Change is calculated as the difference between years 1994–2014 of the historical simulation and years 2080–2100 of the high emissions SSP5-8.5, unless otherwise stated. Our primary focus on SSP5-8.5, which has high cumulative emissions that are unlikely to be reached (Hausfather & Peters, 2020), allows us to maximize the signal of interest. To explore the time periods and scenarios over which these correlations apply, we also calculate relative SLR and PI over years 2014–2100 of the SSP1-2.6, SSP2-4.5 and SSP5-8.5 scenarios for 11 CMIP6 models. These 11 models span the full range of GSAT changes projected by the 26 CMIP6 models used in this study (Figure S1a in Supporting Information S1). The goal of our SLR projections is to produce SLR projections consistent with the GSAT of each model. We note that the methods used to project SLR have considerable uncertainties; however, we choose to choose to focus on the mean projection for each model.

2.1. SLR Projections

2.1.1. Sterodynamic Sea-Level Change

Sterodynamic SLR ($\Delta Z(r)$) is calculated as the linear addition of changes in ocean dynamic sea level ($\Delta\ \zeta$) and global thermosteric sea level (Δh_θ) following Gregory et al. (2019). Sterodynamic SLR and ocean dynamic sea level are local quantities, being a function of two-dimensional geographical location r, specified by latitude and longitude. It can be diagnosed from CMIP6 model variables over time as the sum of the changes in zos ($\Delta\ \zeta(r)$) and zostoga ($\Delta\ h_\theta$):

$$\Delta Z(r) = \Delta\zeta(r) + \Delta h_\theta \tag{1}$$

Dynamic sea level fluctuations, due to regional ocean steric and dynamic effects, are calculated as the local height of the sea surface above the geoid with zero global mean (Gregory et al., 2019), so that it measures sea-level pattern fluctuations around the ocean geoid defined via a resting ocean state at $z = 0$, as defined in Griffies and

Greatbatch (2012) and Griffies et al. (2014). As some models used in this study do not have zostoga output, we calculate h_θ using potential temperature (Text S1.1 in Supporting Information S1).

2.1.2. Antarctic Ice Sheet

To derive future Antarctic Ice Sheet (AIS) dynamical SLR estimates we utilize the impulse response functions by Levermann et al. (2020). Specifically, Levermann et al. (2020) related subsurface ocean warming in Antarctica to projected GSAT change based on an ensemble of CMIP5 models. Estimated basal melt sensitivities from observations were then used to translate subsurface ocean warming into basal ice-shelf loss projections using 16 ice-sheet models that form part of the Linear Antarctic Response Model Intercomparison Project (LARMIP-2).

Following Levermann et al. (2020), we estimate AIS contributions using an linear-response function emulator of the AIS dynamic response to ocean warming for each CMIP6 model. We note that these estimates have considerable uncertainties related to basal ice shelf melt rates, ice sheet models and scaling factors. We convert global barystatic contributions to regional values using the output from a Gravitation, Rotation, and Deformation (GRD) model (Tamisiea & Mitrovica, 2011). The regional imprint of mass loss from the Amundsen sector and the Antarctic peninsula are based on uniform mass loss from West Antarctica. The contribution from East Antarctica and the Weddell and Ross sector is distributed based on the assumption of uniform mass loss from East Antarctica.

In assuming linear response theory, this method neglects any self-dampening or self-amplifying processes. Neglecting self-amplifying processes is particularly relevant in situations in which an instability dominates ice loss, for example, after the onset of Marine Ice Sheet Instability (MISI) and Marine Ice Cliff Instability (MICI; Fox-Kemper et al., 2021; Text S1.2 in Supporting Information S1). These strong caveats that are associated with the approach utilized here, that neglects MISI and MICI, may lead to an underestimation of future dynamical ice loss. Nonetheless, this method provides model specific estimates of Antarctica's future dynamical contribution to SLR.

Following the International Panel on Climate Change (IPCC) Sixth Assessment Report (AR6; Fox-Kemper et al., 2021), we augment LARMIP-2 estimates with surface mass balance (SMB) estimates. As a result of the complex nature of SMB estimation, and the fact that many GCMs tend to overestimate annual precipitation values over ice-sheets, likely due to poor representation of coastal topography (Genthon et al., 2009), this study parameterizes SMB to estimate SLR contributions for the AIS. Parameterizations are derived from relationships between SMB changes and atmospheric temperature using high resolution regional climate models. For each model, we average estimates derived from the parameterizations of Gregory and Huybrechts (2006) and Kittel et al. (2021) to estimate AIS SMB changes (Text S1.2 in Supporting Information S1).

2.1.3. Greenland Ice Sheet

Simulating the changes in continental-scale mass balance (MB) in Greenland Ice Sheet (GIS) models remains challenging due to the small scale of key physics, such as fjord circulation and plume dynamics, and poor understanding of critical processes, such as calving and submarine melting. Fürst et al. (2015) used 10 different CMIP5 AOGCMs simulations to provide MB and ocean forcing for their GIS model, accounting for influences of warming subsurface ocean temperatures and basal lubrication on ice dynamics. We model GIS loss using estimates from Fürst et al. (2015), where GIS MB can be estimated as a cubic function of near-surface temperature anomaly over the GIS (Figure S2 in Supporting Information S1):

$$\Delta MB_{GIS} = 0.03T_{GrIS}^2 - 0.81T_{GrIS} + 2.2 \quad (2)$$

where TAS_{GrIS} is the average anomaly in near-surface temperature over the GIS. As with our AIS projections, our GIS projections omit deeply uncertain process that have the potential to significant increase losses under strong forcing (Fox-Kemper et al., 2021), but these processes are tangential to our study, focused on the correlation between sea-level and TC activity change.

2.1.4. Glaciers and Ice Caps

Over the past century, glaciers and ice caps (GIC) have added more mass to the ocean than the GIS and AIS combined. However, the total remaining mass of glaciers is small by comparison, equivalent to only 0.32 m mean

SLR if only the fraction of ice above sea level is considered (Farinotti et al., 2019). We model GIC following Perrette et al. (2013), where the rate of glacier's ice loss is proportional to a change in GSAT:

$$\frac{dV}{dt} = b_o (T - T_o) \left(1 - \frac{V_{gl}}{V_o}\right)^n \quad (3)$$

where b_o is the global SMB sensitivity, V_{gl} and V_o are the projected and present global glacier volumes (in sea level equivalent) respectively, and n is the scaling coefficient between global glacier area and volume, approximately equal to 1.65 (Perrette et al., 2013). T is the GSAT change as compared to the 1994–2014 historical temperature (T_o). The spatial pattern used here assumes a fixed distribution of the ratios of glacier mass loss between the glacier regions based on the projected distribution in 2100 under Representative Concentration Pathway 8.5 (RCP8.5) (Church et al., 2013; Fox-Kemper et al., 2021). Previous analysis showed that this pattern does not vary much over the 21st century and the mass loss is closely related to the initial glacier mass for a given region. Recent studies have shown that the mass loss distribution is model and scenario dependent (Hock et al., 2019; Marzeion et al., 2020).

2.1.5. Non-Climatic SLR

Changes in land water storage, through groundwater depletion and reservoir impoundment, may have influenced twentieth-century sea-level change but are expected to be relatively minor contributors (Church et al., 2013; Fox-Kemper et al., 2021). We adopt the methods of Kopp et al. (2014) to model land water storage change. Ongoing GIA associated with the adjustment of Earth's lithosphere and viscous mantle material to past changes in ice loading since the last glaciation (e.g., Tamisiea and Mitrovica (2011)) also leaves its imprint in the spatial pattern of sea-level change. This adjustment process gives rise to areas of upward and downward VLM, and the associated mass redistribution also influences Earth's rotation and gravity field with additional impacts on local mean sea level. We use global GIA estimates based on the ICE-6G_C model of Peltier et al. (2015), which uses a wide range of observational constraints, including data from Global Positioning System receivers and time-dependent gravity observations from both surface measurements and the satellite-based Gravity Recovery and Climate Experiment (Argus et al., 2014; Peltier et al., 2015). This data set was sourced from https://www.atmosp.physics.utoronto.ca/~peltier/data.php. We note that non-climatic terms will not contribute to correlations across models, since they are independent of climate forcing and constant across models.

2.2. Large-Scale Factors Known to Modulate TC Activity

Low-resolution AOGCMs (≥100 km grid spacing; Knutson et al. (2020)) are better able to simulate the large-scale environment than individual TCs. Therefore, many studies have chosen to examine large-scale variables known to be associated with TC activity, instead of modeling TCs directly (Camargo, 2013; Emanuel, 2021; Tang & Camargo, 2014; Vecchi et al., 2019). Following Bister and Emanuel (1998), we calculate PI as a function of both the SST and the vertical profiles of temperature and humidity in the atmosphere. Although PI is a prediction only of the maximum intensity that a TC can achieve in a given environment, it is expected to provide a useful guide to the statistical distribution of actual intensities achieved by real TCs (Sobel et al., 2016). Most TCs do not achieve their PI because of a variety of negative influences (e.g., vertical wind shear and ocean cooling effects).

We explore vertical wind shear, with weak vertical wind shear being favorable for hurricane convective organization and intensification (Merrill, 1988; Rios-Berrios & Torn, 2017). Vertical wind shear is calculated as the magnitude of the vector difference of wind velocity at 850 and 200 hPa, computed from monthly mean output. Increases in PI and decreases in vertical wind shear suggest an environment more conducive to future TC activity (Bister & Emanuel, 1998; Emanuel, 2013; Emanuel & Nolan, 2004).

2.3. Hydrodynamic-Climatological Modeling

Storm tide (combination of astronomical tide and storm surge) projections are based on simulations of Gori et al. (2022), using the 2D depth-integrated version of the hydrodynamic model ADvanced CIRCulation (ADCIRC; Luettich et al., 1992; Westerink et al., 1994). We model storm tides for each of the eight CMIP6 models (herein ADCIRC-CMIP6 models) that overlap with the study of Gori et al. (2022) (see Figure 4 for the models) for the simulations employed in this study. TCs are modeled using the statistical-deterministic hurricane

model developed by Emanuel et al. (2008) and Emanuel (2021). The ADCIRC mesh has a resolution of between 1 km nearshore and 100 km in the deep ocean (Gori et al., 2022; Lin et al., 2019; Marsooli et al., 2019). We assume the cyclone-threatened area for each site to be within a 200-km radius.

Statistical analysis is performed on the modeled peak storm tides to produce return period curves for each model. Flood return periods presented here are bias-corrected by comparing National Centers for Environmental Prediction (NCEP) based storm tide reanalysis for the historical period with model-based estimates on TC intensity for the same historical period and assuming the same bias in the future period. Assuming that the storms arrive as a stationary Poisson process under a given climate, the return period of TC-induced storm tide height (H^f) exceeding a given level h is (Lin et al., 2016):

$$T_{H^f}(h) = \frac{1}{\lambda\,(1 - P\,\{H^f \le h\})} \tag{4}$$

where $P\{H^f \le h\}$ is the cumulative probability distribution (CDF) of peak storm tide level and λ is the annual TC frequency. Extreme events usually produce rare, long tail probability distribution events. Here, we model the tail of the storm tide CDF using the Peaks-Over-Threshold method with a Generalized Pareto Distribution and maximum likelihood estimation (Coles, 2001). Non-parametric density estimations are used to model the rest of the distribution. We determine the tail threshold value by trial and error so that the smallest error in the distribution fitted to the tail is obtained.

3. Results

3.1. Future SLR and Factors Affecting TC Activity

We present the CMIP6 ensemble mean relative SLR as a difference between years 1994–2014 of the historical simulation and years 2080–2100 of the SSP5-8.5 simulation (Figure 1a). Median GMSLR is 0.68 m, slightly larger than the AR6 estimate of 0.64 m (17th–83rd percentile ranges of 0.52–0.83 m) in 2090 (Fox-Kemper et al., 2021), with projections across the ensemble positively correlated with GSAT change ($\rho = 0.82$; Figure S3a in Supporting Information S1). Note that, because all the models are driven by a single emissions scenario, this spread in GSAT is entirely due to between-model differences in climate sensitivity. Our ensemble estimates of GIC (0.16 m), thermal expansion (0.26 m) and GIS (0.1 m; Figure S4 in Supporting Information S1) are consistent with respectively values reported in AR6 of 0.15 m, 0.25 and 0.1 m in 2090 (Fox-Kemper et al., 2021).

Under the high-emissions scenario (SSP5-8.5) studied here, 21st century SLR scales with regional temperature change at approximately 0.15 and 0.14 m per degree in the western North Atlantic and North West Pacific, respectively (Figures 1d and 1g; regions defined in Figure 1a). Global mean sea level rise also scales with GSAT change increase at an average rate of 0.11 m per degree across the ensemble. Relative SLR in the western North Atlantic and North West Pacific exceeds the global mean rate in part due to regionally high sterodynamic changes and as a consequence of the higher than global mean barystatic SLR associated with the spatial GRD fingerprints (Figures S5a–S5d). We note that future barystatic contributions to SLR may not scale with GSAT, as MISI and MICI, not modeled here (see Section 2.1), have the potential to cause non-linear increases in SLR with GSAT changes (Deconto et al., 2021; Fox-Kemper et al., 2021).

Whilst the CMIP6 ensemble mean June–November PI increases over most of the northern hemisphere tropics, there is a large region in the northern tropical Atlantic where the ensemble-mean PI decreases (Figure 1b). Projections of PI in CMIP3 (Vecchi & Soden, 2007a, 2007c) and CMIP5 models (Camargo, 2013; Sobel et al., 2016) have very similar patterns in the Northern Hemisphere to that shown here. In agreement with Vecchi and Soden (2007a); Vecchi and Soden (2007c), we find that PI changes around the globe closely follow the structure of SST changes—with regions that warm more (less) than the tropical mean (relative SST; averaged over 35°S–35°N) showing a PI increase (decrease; Figure 1b). CMIP6 models project an average PI increase of 4.5% and 5.2% per degree regional temperature warming in the western North Atlantic and North West Pacific, respectively (Figures 1e and 1h). Globally averaged PI increases at a rate of 2.3% per degree GSAT warming, consistent with an increase of 5% (likely range 1%–10%) per two degrees warming as estimated in Knutson et al. (2020).

Using a subset of CMIP6 models, Hermans et al. (2021) found that global mean sea level (GMSL) scales with integrated GSAT, with most of the contributors to GMSL being more closely tied to time-integrated GSAT than

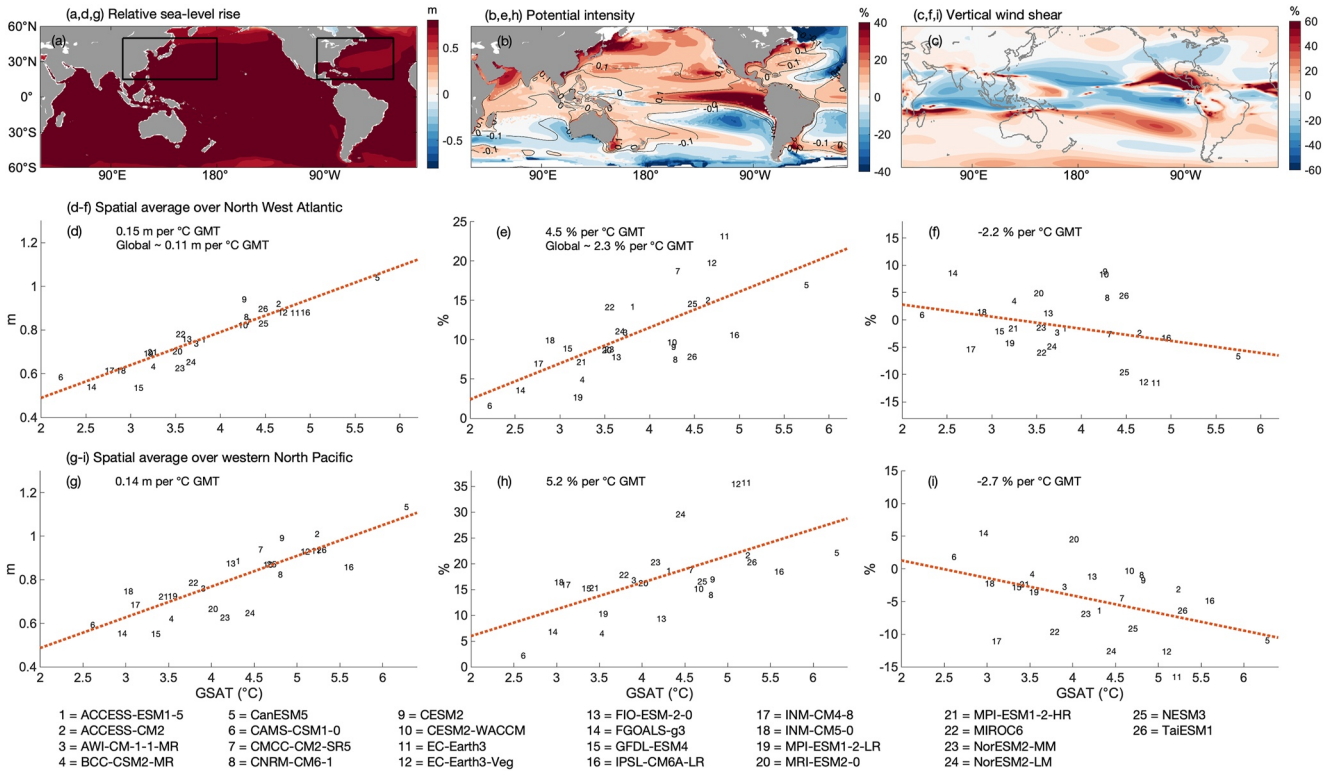

Figure 1. Panels (a–c) show the ensemble mean response of relative sea-level rise (a), potential intensity (PI) (b) and vertical wind shear (c). PI and vertical wind shear are displayed as percentage increases from years 1994–2014 of the historical simulation. Anomalies in PI and vertical wind shear in the Northern Hemisphere are computed over June through November, while anomalies in the Southern Hemisphere are computed over December through May. Contours in (b) show the normalized departure of the local SST change from the tropical-mean (averaged over 35°S–35°N) SST change. Scatter plots show the spatial averages over the western North Atlantic (d–f) and North West Pacific (e–i): Each dot represents a single model. The solid black boxes in (a) show the North West Pacific and western North Atlantic regions.

instantaneous GSAT, meaning that sea level projections can only be interpreted if the warming levels are linked to a specific time-frame (Fox-Kemper et al., 2021). In contrast to GMSL, using a subset of CMIP6 models, we find that globally averaged PI appears to scale with instantaneous GSAT in a time- and scenario-independent manner (Figure S6 in Supporting Information S1). Thus, the rates of increase in PI per degree GSAT change found here will likely be constant regardless of time or emissions scenario.

Basin-specific changes in vertical wind shear are projected, with increases across the tropical Atlantic and decreases across the northern tropical Pacific and western North Atlantic (Figure 1c). The CMIP6 model mean pattern is similar to that obtained in CMIP3 (Vecchi & Soden, 2007c) and CMIP5 (Camargo, 2013; Ting et al., 2019) models for the Northern Hemisphere TC season. These changes in vertical shear are associated to the projected decrease in the Pacific Walker circulation (Vecchi & Soden, 2007c), while the near-equatorial vertical shear weakening reflects a reduction of zonal overturning (Vecchi & Soden, 2007b, 2007c).

Projected changes to vertical wind shear over the ocean in the western North Atlantic and North West Pacific are −2.2% and −2.7% per degree regional temperature warming, respectively (Figures 1f and 1i). Reducing vertical wind shear in these regions is consistent with the expected expansion of the Hadley circulation (Lu et al., 2007; Kang & Lu, 2012), and the related northward shift of the midlatitude jet stream (Ting et al., 2019). To determine the change in vertical wind shear due to contributions from the upper and lower levels, Figure 2 shows the wind vector differences between the two periods. The intensification and northward shift of the midlatitude jet is clearly seen at both the upper and lower levels in the Atlantic and the Pacific, being stronger and more defined in models that project higher GSAT warming (Figures 2c and 2f). In agreement with a similar analysis of CMIP5 models (Ting et al., 2019), there is some indication of a southward flow at the lower level and northward flow at the upper level, implying an enhanced and northward extended Hadley circulation (Figure 2).

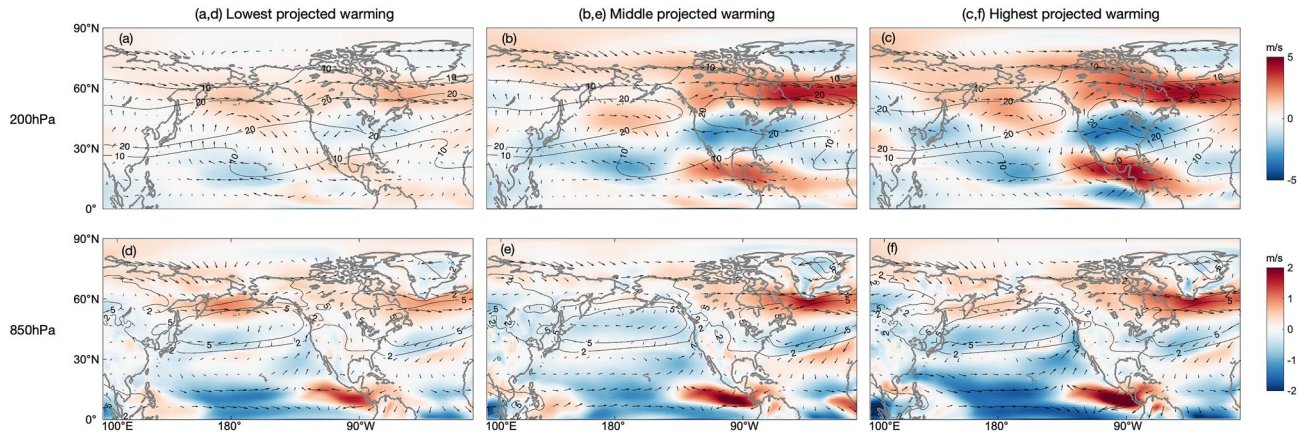

Figure 2. Composites of June-November mean 200 hPa (top) and 850 hPa (bottom) horizontal wind vector differences between the average for the SSP5-8.5 (2080–2100) and the historical period (1994–2014). Background colors show speed changes and contours show historical zonal winds. Composites are based on projected global mean surface air temperature (GSAT) warming (a,d) Lowest project warming being the average over the models with the lowest third of projected GSAT change (c,f) highest projected warming models being the average over the top third of project GSAT changes. Anomalies are computed over June through November.

Large inter-model differences exist: the CMIP6 model with the highest GSAT change (CanESM5; GSAT of 7.0°C) projects a GMSLR of 0.98 m and a 14% increase in globally averaged PI, whereas, the model with the lowest GSAT (CAMS-CSM1-0; GSAT of 2.8°C) projects a GMSLR of 0.61 m and an 4% increase in globally averaged PI (Figure S3). Inter-model spread is strongly related to GSAT change, which is positively correlated to GMSLR ($\rho = 0.82$) and globally averaged PI ($\rho = 0.62$; Figure S3 in Supporting Information S1). Additionally, models fall roughly at the same position in the CMIP6 ensemble SLR and PI change distributions in the western North Atlantic when compared to the North West Pacific (e.g., CAMS-CSM1-0 projects the lowest average relative SLR and PI change in both regions; Figure 1), suggesting that changes are coupled and are related by global mean changes.

Hence, in CMIP6 models, GMSLR and global mean PI change are closely related to GSAT change, whilst spatial patterns in PI change are tightly coupled with spatial changes in relative SST. Vertical wind shear tendencies are spatially more complex. In the western North Atlantic and North Pacific, vertical wind shear responds to changes in the mid-latitude jet, which is generally stronger in CMIP6 models that project higher GSAT change. As the climate system is strongly coupled, global and regional co-variability between SLR and TC activity, shown here to be related to GSAT change, may impose correlations between these variables. We next explore these correlations.

3.2. Correlation Between SLR and Large Scale Factors Affecting TCs

The inter-model correlation is computed as the rank correlation across the CMIP6 ensemble between SLR and TC activity in historical and future (SSP5-8.5) simulations (Figure 3). There are strong positive correlations between PI change and relative SLR in most regions: models with large PI increases show higher projected relative SLR (Figure 3a). This strong SLR-PI relationship is consistent with both being broadly related to GSAT change (see Section 3.1). To explore the time periods and scenarios over which these correlations apply, we calculate intra-model correlations between relative SLR and PI change (Figure S7 in Supporting Information S1). Intra-model correlations are calculated over the full 86 years of the SSP1-2.6, SSP2-4.5 and SSP5-8.5 scenarios for 11 CMIP6 models. The spatial patterns of intra-model correlations are very similar across scenarios, however, the correlation coefficients are stronger over time and in the higher emissions scenarios (Figure S7 in Supporting Information S1). The reason for this difference may be due to larger ratio of forced signal to internal variability for later time period and for higher emissions scenarios. Sea-level rise contributions from land ice loss are strongly correlated with PI and vertical wind shear change in the western North Atlantic and North West Pacific (Figures 3e–3j). Sea-level rise from land ice loss follows the spatial patterns of GRD fingerprints that is constant across models, meaning that the spatial correlations between TC activity and barystatic SLR are a result of common relations to global mean changes, rather than as a result of regional co-variability.

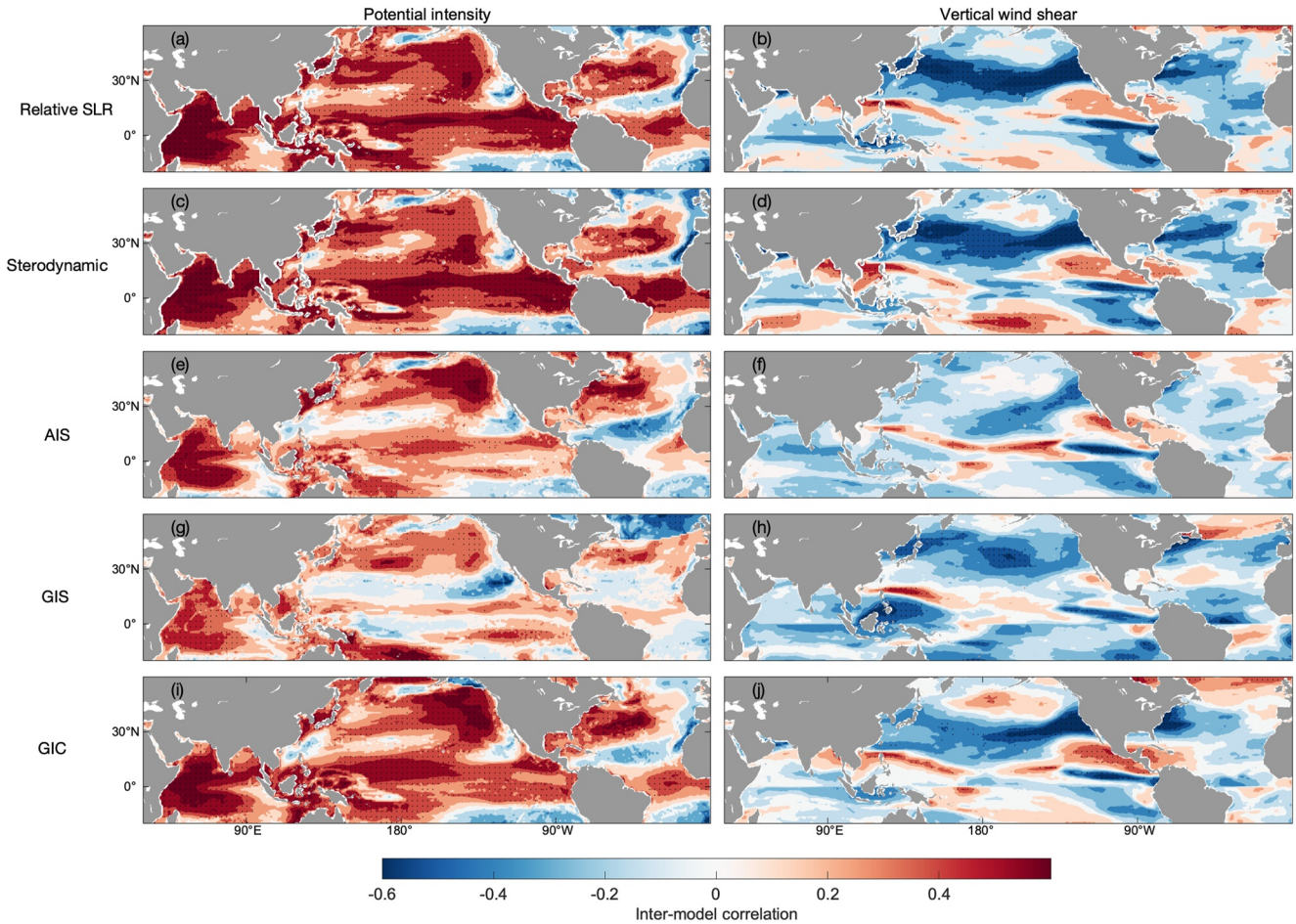

Figure 3. Inter-model correlations between sea-level rise (SLR) (rows) and potential intensity (left column) and vertical wind shear (right column) for all 26 CMIP6 models. Rows show each component of SLR: Relative SLR (a–b), sterodynamic (c–d), Antarctic (e–f), Greenland (g–h) and Glaciers and Ice caps (i–j). Stipples denote correlations significant to 95%.

Relative SLR and vertical wind shear show regionally variable inter-model correlations (Figure 3b), that largely follows the spatial pattern of the ensemble mean vertical wind shear change (Figure 1c), being strongly negative in the western North Atlantic and North West Pacific, whilst positive in the tropical Atlantic region. As relative SLR increases in all low latitude regions (Figure 1a), the spatial pattern of correlations generally follows the spatial patterns of mean state changes in PI and vertical wind shear (Figures 3a and 3b). Additionally, we find that PI and vertical wind shear are negatively correlated in parts of the western North Atlantic and North West Pacific (Figure S8 in Supporting Information S1). The projected weakening of the vertical wind shear environment in the western North Atlantic and North West Pacific may help TCs reach their PI into the future. As PI and vertical wind shear are anti-correlated over much of the western North Atlantic and North West Pacific (Figure S8 in Supporting Information S1), based solely on these metrics, we may well expect a non-linear increase in TC intensity.

The increases in PI across the western North Atlantic and North West Pacific, coupled with the more favorable vertical wind shear change suggests a large scale environment more conducive to TC intensification, with TCs having a better chance of achieving higher PIs in these regions (Ting et al., 2019). Additional and concurrent increases in relative SLR, suggest a significant and compounding intensification of flood hazard in these regions, based solely upon these metrics. For the Gulf Coast and tropical Atlantic, the future projected increase in vertical wind shear may induce a reduction of the intensity of strong landfalling TCs, although the increase in PI there may outweigh the effect of increasing vertical wind shear.

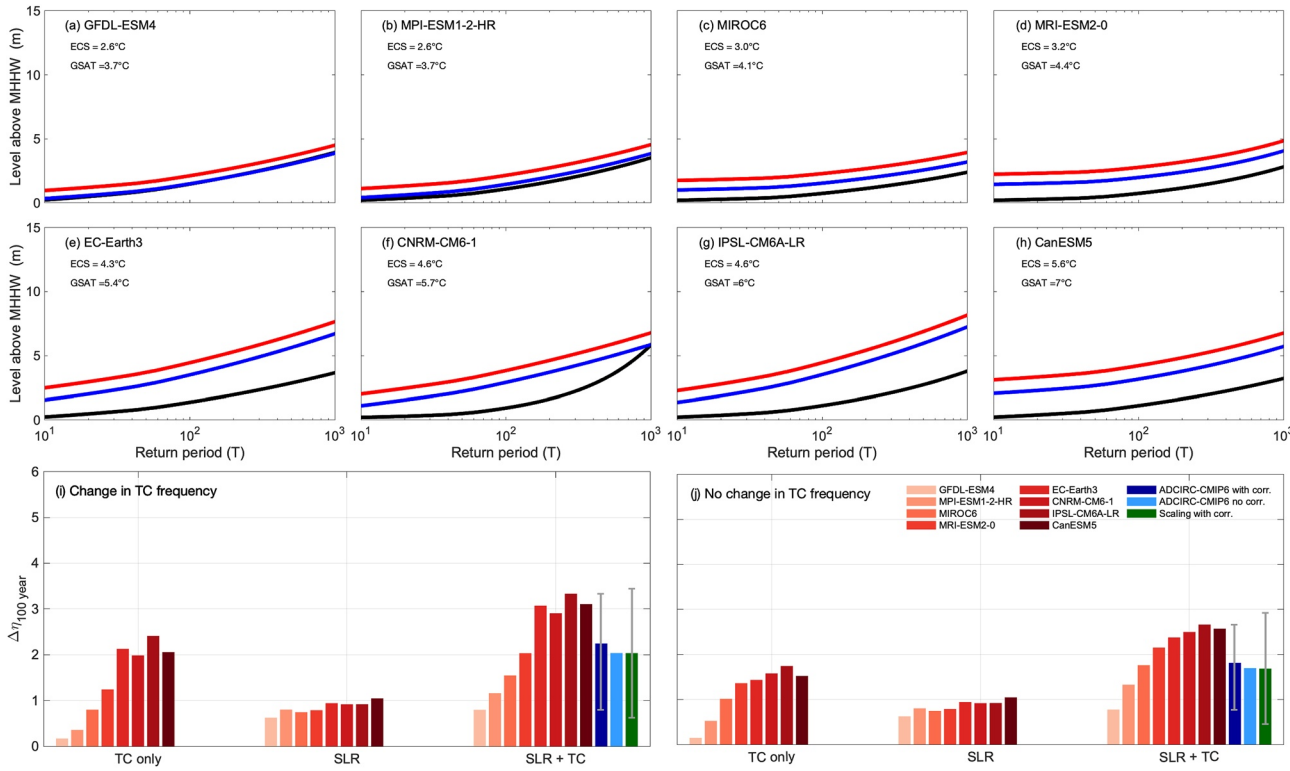

Figure 4. Estimated storm tide return levels for the historical period (black) and future period of 2080–2100 (blue: only effects of tropical cyclone (TC) changes, red: Compound effects of sea-level rise [SLR] and TCs) at Wilmington, NC (a–h). Models are ordered by ascending effective climate sensitivity. Bar charts show the contributions of SLR and TC change to the change in the 100 years historical storm tide level, assuming (i) change and (j) no change in TC frequency at Wilmington, NC. Storm tide levels are relative to mean higher high water (MHHW, obtained from https://vdatum.noaa.gov). The dark blue bars on (i–j) show the mean of the ADICRC-CMIP6 models that includes correlated changes, whilst the light blue bars show the ADCIRC-CMIP6 projection constructed through convolution (i.e., neglecting correlations). The green bars on (i–j) show the compound changes derived from the scaling method based on the global mean surface air temperature and SLR projections of all 26 Coupled Model Intercomparison Project Phase 6 models as described in Section 3.3.3. Vertical gray bars (i–j) denote the model ranges.

We have found strong inter- and intra-model correlations between SLR and TC activity change, with GSAT change being the key physical mechanism driving co-variability (Section 3.1). The correlations between TC activity and relative SLR, may in turn affect the occurrence frequency and intensity of multivariate extreme events along the coast. We next explore the extent to which joint changes impact future coastal flood events at five sites along the US East Coast, focusing on Wilmington, NC as an example.

3.3. Implications for Coastal Flooding

3.3.1. Future Changes to the Storm Tide at Wilmington

Synthetic TCs used in this study are generated in Gori et al. (2022) for the US East and Gulf Coasts using the statistical-deterministic hurricane model of Emanuel et al. (2008) and Emanuel (2021). The TC model generates synthetic TCs for a given large-scale atmospheric and oceanic environment. Figure 4 presents the estimated storm surge return levels projected under the future climate, compared with those of the historical period, for Wilmington, NC. In agreement with prior studies (Gori et al., 2022; Marsooli et al., 2019; Marsooli & Lin, 2020), the storm tide level for a given return period substantially increases by the end of 21st century, due to relative SLR as well as TC climatology change. To quantify future flood hazard, we focus on the change in the 100-year storm tide level ($\Delta\eta_{100}$). Our projections show an increase of between 0.8 and 3.3 m, with an average increase of 2.2 m (Figure 4j and Table 1).

The increase in $\Delta\eta_{100}$ for each model at Wilmington is evidently related to each model's GSAT change and effective climate sensitivity (ECS; Figures 4a–4h and Table 1). For example, changes to the $\Delta\eta_{100}$ for GFDL-ESM4 (GSAT = 3.7°C) is 0.8 m (TC only = 0.18 m; SLR only = 0.62 m). For CanESM5 (GSAT = 7.0°C) the projected

Table 1
Projected Changes in Relative Global Mean Surface Air Temperature (GSAT) (°C), $\Delta\eta_{100}$ (m), Sea-Level Rise (SLR) (m) and Tropical Cyclone Characteristics at Wilmington, NC for the Coupled Model Intercomparison Project Phase 6 Subset Modeled With ADvanced CIRCulation

Model	GSAT (°C)	$\Delta\eta_{100}$ (m)	SLR (m)	Annual frequency	RMW (%)	PI (%)	TS (%)
GFDL-ESM4	3.7	0.8	0.62	0.2	−11	9.2	−10
MIROC6	4.1	1.2	0.80	0.75	−10	14	−5.2
MPI-ESM1-2-HR	3.7	1.5	0.74	0.34	−9.3	8.1	−9.8
MRI-ESM2-0	4.4	2.0	0.79	0.2	−19	18	−16
EC-Earth3	5.4	3.1	0.94	4.4	−22	43	−25
CNRM-CM6-1	5.7	2.9	0.91	1.3	−14	29	−10
IPSL-CM6A-LR	6	3.3	0.92	3.1	−18	43	−25
CanESM5	7.1	3.1	1.0	0.34	−15	22	−24

Note. RMW, potential intensity (PI) and TS denote the changes in the radius of maximum wind speed, maximum wind speed and translation speed, respectively. Change is calculated as the difference between years 1994–2014 of the historical simulation and years 2080–2100 of the high emissions SSP5-8.5.

increase is 3.1 m (TC only = 2.1 m; SLR only = 1.0 m; Figure 4i). Importantly, relative SLR and TC climatology change generally both increase in a concurrent manner with GSAT change across models. The difference in projected $\Delta\eta_{100}$ between the models with the lowest (GFDL-ESM4) and highest (CanESM5) projected GSAT change, incorporating each models own relative SLR and TC change, is as large as 2.3 m at Wilmington by 2080–2100 (Figure 4i).

In our simulations, changes to storm frequency for Wilmington are large in the future (Table 1). As TC frequency is a major uncertainty in the projections of TCs (Knutson et al., 2020), we repeat our analyses assuming that there is no change in annual frequency (Figure 4j). By neglecting changes in TC frequency, projected TC storm surge changes are substantially reduced at Wilmington, with models that projected low GSAT change now projecting little change to TC storm tides (Figure 4k). We still, however, find evidence of concurrent increases in TC surge with relative SLR and GSAT change at Wilmington. For example, CanESM5 projects an increase of $\Delta\eta_{100}$ of 2.3 m (TC only = 1.3 m; SLR only = 1.0 m), whilst GFDL-ESM4 projects an increase to the $\Delta\eta_{100}$ of 0.77 m (TC only = 0.15 m; SLR only = 0.62 m). Changing storm tide levels even when frequency is held constant, suggests that TC intensity, track, size and translation speed will change by the end of 21st century. We next explore these metrics.

3.3.2. Changing TC Characteristics

We find that the TC track exhibits change into the future, with some evidence of a shift away from the US East Coast into the future denoted by a greater increase in TC density parallel to the coast, particularly in the mid-Atlantic region (Figure 5a) in general agreement with prior studies (Garner et al., 2017, 2021; Marsooli & Lin, 2020). However, in contrast to Garner et al. (2017), the shift in track is not large enough to keep TC storm surge magnitude constant into the future. The movement of TCs tracks is predominately determined by the steering winds, with modifications due to the beta effect (Chan, 2005), the former being strongly related to the position and strength of the subtropical highs. In general agreement with CMIP3 (26 models in Li et al. (2012)) and CMIP5 models (13 models in Li et al. (2013) and 20 models in Camargo (2013)), we find a significant intensification of the North Atlantic subtropical high (Figures 5b–5c), which has been related to an increase in thermal contrast between the land and ocean (Li et al., 2012). CMIP6 models mean sea-level pressure (SLP) differences indicate that future SLP is significantly higher (100 Pa) over the North Atlantic Ocean and lower over the United States (Figures 5b–5c). Additionally, mean SLP differences of all 26 CMIP6 models suggest a more westward pattern in the North Atlantic subtropical high compared to the ADCIRC-CMIP6 subset (Figure 5c).

The flooding potential, and to some extent the wind damage, caused by TCs can be strongly affected by their translation speed. Slower TCs allow winds to blow onshore for longer periods of time, resulting in possibly larger and longer coastal flooding. Our analysis of TC translation speed and intensity (maximum wind speed) also reveals an increase in the number of slow-moving and stronger TCs along the US East Coast (Figures 6a

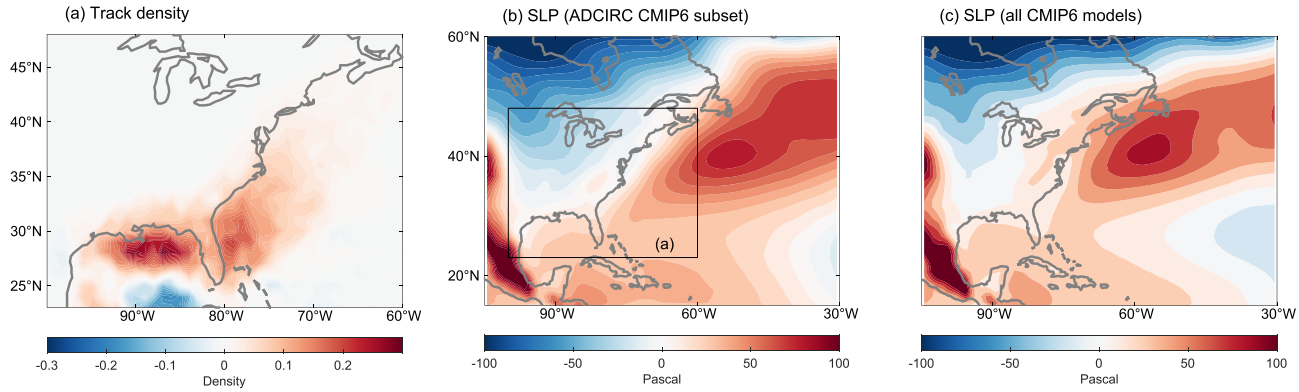

Figure 5. Multimodel mean difference between future and modern synthetic tropical cyclone (TC) track densities assuming no change in TC frequency (a). Track densities are determined by the sum total of tracks crossing through each grid box over 20-year periods from 2080–2100 and 1994–2014, divided by the area of that grid box and the number of years (b,c) Mean sea-level pressure differences (pascals) averaged over June–November for the eight Coupled Model Intercomparison Project Phase 6 (CMIP6) modeled with ADCIRC (b) and for all 26 CMIP6 used in this study (c).

and 6b), consistent with Garner et al. (2021). At Wilmington, models that project higher GSAT change and relative SLR, project considerably slower and more intense TCs than low GSAT change models (Table 1). For example, synthetic TCs derived from CanESM5 suggest mean changes to TC intensity and translation speed of 22% and −24% respectively, whilst GFDL-ESM4 projects changes of 9.2% and −10% (Table 1).

We utilize the complete wind profile of Chavas et al. (2015) to estimate the radius of maximum wind speed, where projected decreases in radius of maximum wind speed are consistent with increases in maximum wind speed, assuming constant TC outer sizes (Chavas et al., 2016; Knutson et al., 2015). As TC intensity is projected to increase, we find that this wind model projects a decrease in radius of maximum wind speed along the US East Coast (Figure 6c).

We also explore inter-model correlations between relative SLR and projected changes in TC characteristics (Figures 6d–6f). Relative SLR is positively correlated with TC intensity, and negatively correlated with

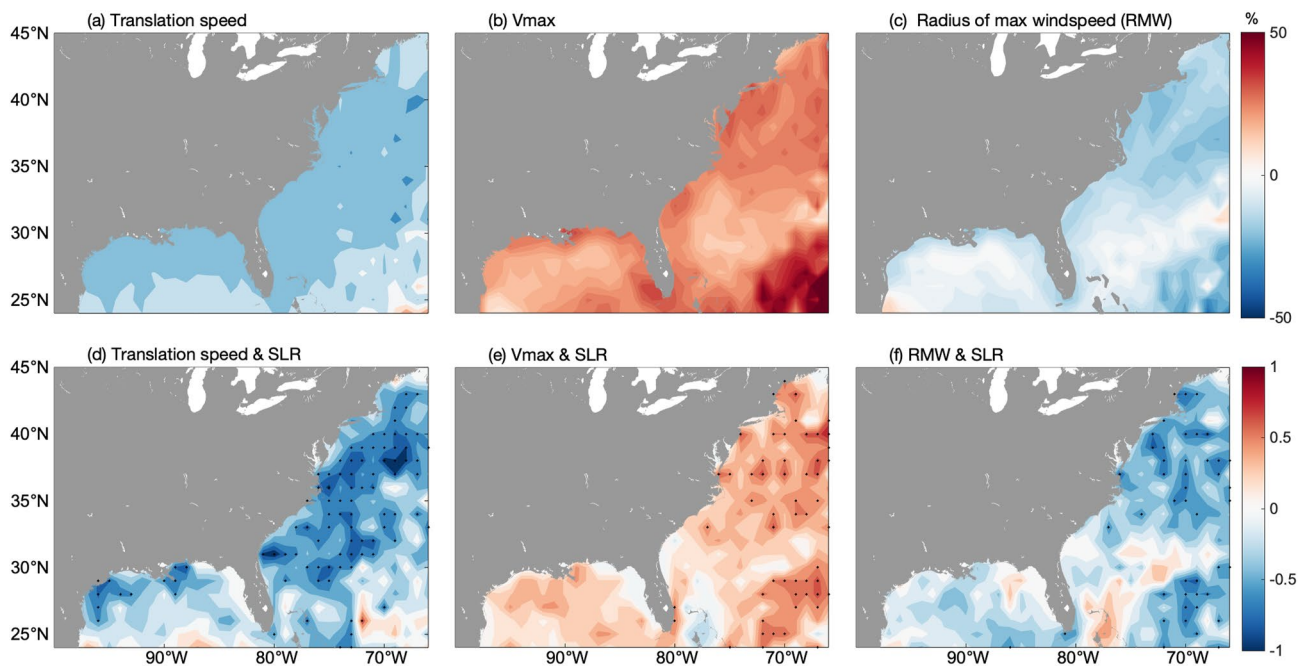

Figure 6. (a–c) Multimodel mean projected changes in translation speed, tropical cyclone (TC) intensity and radius of maximum wind shown as percentage increases from years 1994–2014 of the historical simulation (d–f) Inter-model correlations between projected changes in TC characteristics and relative sea-level rise.

Table 2
First and Second Columns Show the $\Delta\eta_{100}$ Including and Excluding Correlations Between Sea-Level Rise and Tropical Cyclone Surge Distributions, Respectively

Location	$\Delta\eta_{100}$ correlation (m)	$\Delta\eta_{100}$ no correlation (m)	Change (%)	Selection bias (%)
New York City, NY	1.6	1.5	6	−8.2
Wilmington, NC	2.5	2.2	12	−7.1
Charleston, SC	2.9	2.5	14	−8.1
Miami, FL	1.94	1.9	2	−7
New Orleans, LA	3.5	3.1	12	−7.8

Note. The third column shows the percentage change (%) when correlations are included. The last column shows the change in mean storm tide value when selection bias is included.

translation speed and radius of maximum wind speed along most of the US East Coast and Gulf of Mexico. Based on these correlations, we can deduce that compounding of increased flood hazard at Wilmington with relative SLR and GSAT warming will likely be driven by stronger and slowing moving TCs and possibly their increased frequency, that may be counteracted in part by TCs with smaller radius of maximum wind speed.

3.3.3. Implications for Coastal Flood Modeling

We have found that relative sea levels and TC storm surges both increase strongly with GSAT warming at Wilmington, NC. In this section, we evaluate (a) the extent to which studies misrepresent future flood hazard by assuming that the TC storm surge and SLR distributions are uncorrelated and (b) the impact of model selection bias on projected changes to flood hazard. To explore (a), we compare the ADCIRC-CMIP6 projection that includes correlated changes (dark blue bars on Figures 4i–4j) with the ADCIRC-CMIP6 projection that neglects correlated changes (light blue bars on Figures 4i–4j). Flood hazard projections that neglect correlated changes are calculated through the convolution of the entire ADCIRC-CMIP6 storm tide and SLR distributions, which assumes that the two distributions are statistically independent. Flood hazard projections that include correlated changes are calculated by combing each model's own SLR and TC projections (dark blue bars on Figures 4i–4j). We find that by neglecting positive correlation between SLR and TC surge change, the projection of $\Delta\eta_{100}$ is under-estimated by 0.26 m (12%) and 0.14 m (8%) assuming frequency changes and no frequency change, respectively.

As joint variability between SLR and TC change is modulated by GSAT change, selection bias in GSAT may substantially alter the projected change in flood hazard at Wilmington. For example, the ADCIRC-CMIP6 models are negatively skewed in GSAT projections compared to the distribution of all 26 CMIP6 models (three are in the top 25%; Figure S1b in Supporting Information S1), which in this instance, may be leading to overly strong projections of compound changes at Wilmington. To explore potential selection bias, that is, selection that doesn't obtain a sample representative of all GSAT projections, we compare the ADCIRC-CMIP6 projection that includes correlated changes (dark blue bars on Figures 4i–4j) with a simple scaling relationship between ADCIRC-CMIP6 TC climatology change and GSAT change, that is applied to the projections of all 26 CMIP6 models (green bars on Figures 4i–4j). At Wilmington the $\Delta\eta_{100}$ due to TC climatology change increases at a rate of 0.27 m (lowest 0.2 m; highest 0.34 m) and 0.1 m (lowest 0.05 m; highest 0.19 m) per degree GSAT change assuming frequency changes and no frequency change, respectively (Figure S9 in Supporting Information S1). We apply these scaling relationships to the GSAT and relative SLR projections of all 26 CMIP6 models. Specifically, we randomly sample one of the eight scaling factors (from the eight ADCIRC-CMIP6 models) and apply it to a randomly selected one of the 26 CMIP6 models based on its GSAT and add its SLR projection 100,000 times. By comparing this scaling estimate (green bar on Figures 4i–4j) with the ADCIRC-CMIP6 projection that includes correlated changes (dark blue bar on Figures 4i–4j), we find that selection bias is leading to an over-estimated average projection of $\Delta\eta_{100}$ of 0.15 m (7%) and 0.1 m (6%) assuming frequency changes and no frequency change, respectively (Figures 4i–4j).

We repeat these analyses for Miami, New York, Charleston and New Orleans (Table 2). We find that selection bias is fairly consistent across locations, leading to an over-estimation of flood hazard by between 7.1% and 8.2%. We find that the impact of correlations varies strongly with location, with positive correlations leading to a substantial increase in mean $\Delta\eta_{100}$ at Charleston (14%), Wilmington (12%) and New Orleans (12%). In contrast, at New York and Miami, correlations lead to an increase in mean $\Delta\eta_{100}$ of 6% and 2%, respectively. The impact of correlations on flood hazard shows some relation to the spatial correlations between SLR and TC characteristic changes (Figures 6d–6f) and to track changes (Figure 5a). For example, the small impact of positive correlations on $\Delta\eta_{100}$ at Miami may be a result of weak correlations between SLR and synthetic TC translation speed, Vmax and RMW at this location (Figures 6d–6f). The small impact of positive correlations on $\Delta\eta_{100}$ at New York City, may be a result of an evident shift offshore of the TC track at this location (Figure 5a). At Charleston, Wilmington and New Orleans, however, there are strong correlations between SLR and TC characteristics and substantial increases in track density at these locations (Figure 5a).

We have found that by focusing on a subset of AOGCMs that do not reflect the full distribution of GSAT changes within the emission scenario, and by assuming independence between SLR and storm tide change, coastal flood hazard assessments may not accurately capture future coastal flood hazard. We recommend that future studies that focus on a specific emissions scenario: (a) construct SLR and TC projections inherent to each model to ensure that correlations are incorporated, (b) consider extremes as well as average projections, given that model variation is strongly modulated by joint variability related to GSAT and (c) be mindful of the GSAT change and ECS of each CMIP6 model used, as selection bias may substantially alter flood hazard projections.

4. Discussion

The results of this analysis indicate that flood hazard in the western North Atlantic and North West Pacific will increase substantially over the twenty first century due to relative SLR, compounded by TC climatology change. Effects on flooding of correlations exhibits substantial spatial heterogeneity, likely related to changes in TC track density and to spatial patterns in correlations between SLR and synthetic TC characteristics. For Wilmington, where strong correlations are evident between SLR and TC characteristics, neglecting correlated changes results in the average projected change to the historical 100-year flood level being under-estimated by 12%. At Miami, FL, where there are weak correlations between SLR and TC characteristics, neglecting correlations leads to an under-estimation of average $\Delta\eta_{100}$ by 2% (Table 2). While including correlation leads to a correction that is modest compared with the total storm tide in these cases, the values at Wilmington are large enough to merit attention from coastal planners and engineers planning future protection policy and measures.

We also treat storm tides and SLR as linearly additive. This is problematic because interactions between SLR and surge and tides can potentially create a bias, up to the order of 15% in the future flood elevation, either high or low depending on exact geographic location (Resio & Irish, 2015). Although future SLR-TC interactions are expected to be small at NYC (Lin et al., 2010, 2012), studies have found that interactions can be large within some bays and estuaries (Bilskie et al., 2016, 2020). Correlations between SLR and TC storm surge may also impact SLR-TC surge interactions; if changes to both SLR and TC storm surges are large then interactions between these components may also be stronger, further impacting future flood hazard.

SLR and future TC activity will respond to radiative forcing, atmospheric feedbacks, the horizontal and vertical distribution of oceanic and atmospheric warming, and changes in climate oscillations, amongst others (Little et al., 2015; Woodruff et al., 2013). As the climate is a strongly coupled system, regional changes in climate forcing may be co-dependent (Lambert et al., 2021); and it is this co-dependence that imposes correlations between SLR and TC activity and associated coastal flooding. In this analysis, we do not attempt to rigorously explain correlations across the ensemble, as an individual model's response may be a combination of multiple drivers that have not been considered here. More efforts to clarify causal mechanisms and role of uncertainties are required to constrain the timescales and radiative forcing scenarios over which these correlations apply. Additionally, although our results focus on years 2080–2100 of SSP5-8.5, which has unrealistically high anthropogenic carbon dioxide emissions (Hausfather & Peters, 2020), strong correlations are evident in SSP2-4.5 and earlier in the 21st century and that may also impact flood hazard assessments (see Section 3.2).

We also note that our results may be influenced by model selection bias, resulting from the fact that not all CMIP6 model output is available. To explore this, we compare GSAT projections of models used this study (26 models) to all available CMIP6 models that have surface temperature (tas) for the simulations and run used (34 in total; Figure S1c in Supporting Information S1). The 26 CMIP6 models used here, span the full range of projected GSAT change, giving us some confidence that our results should be largely unaffected by the addition of other CMIP6 models. In addition, our results rely on a number of land ice SLR parameterizations that have considerable uncertainty. Ideally, our methodology would be applied to explicit model projections of all sea-level components, rather than parameterizations.

As the model uncertainty contributes a large portion of the total projection uncertainty in SLR and TC activity, uncertainties may be reduced if outlier models can be shown to be unreliable (Little et al., 2015). In particular, our results indicate that the divergent behavior of CMIP6 models in projections of future TC activity and relative SLR, is driven by models that project high ECS. Some high ECS models used in this study project more positive cloud feedback in response to increasing green-house gases, and they also tend to have a stronger cooling effect from aerosol-cloud interactions (ACI) when compared to low ECS models (Wang et al., 2021). These strong

effects in the high ECS models offset each other during much of the 20th century, when both anthropogenic aerosols and emissions increased. However, these high ECS models poorly simulate the spatial pattern of historical warming compared to low ECS models as aerosols are concentrated in the Northern Hemisphere (Wang et al., 2021).

The compensating affects of strong ACI and cloud feedback in the high ECS models, which occurs over the historical period, does not occur into the future, as aerosols are projected to decrease as greenhouse gases rise. CMIP6 models with more positive cloud feedback, as a result, tend to have higher 21st century projected warming (Brunner et al., 2020), ECS (Wang et al., 2021), and therefore, potentially higher SLR and future TC activity. Indeed, we find that CMIP6 models that project the highest GMSLR and globally averaged PI in this study also project the highest ECS and strongest cloud feedback (Figure S10 in Supporting Information S1). If these high ECS and cloud-feedback models, which poorly simulate the spatial pattern of historical warming, can be shown to be unrealistic, substantial uncertainty reductions in projections (that are derived directly from CMIP6 models) of TC activity and SLR, could result.

Finally, rain rates near the centers of TCs are also expected to increase with increasing global temperatures (Knutson et al., 2015, 2020). The amount of TC related rainfall that any given local area will experience is proportional to the rain rates and inversely proportional to the translation speeds of TCs (Kossin, 2018). Our projections of slower moving storms along the US East Coast may therefore contribute to an increased rate of rain in TCs in some regions (Gori et al., 2022). In the northeast region of the United States, especially in New England, coastal flooding induced by extra-tropical cyclones (ETCs) are more frequent (but less destructive) than TC-induced flooding (Booth et al., 2016). The effect of climate change on ETC storm surges is thought to be relatively small on average along the US East Coast, although large uncertainties exist among climate models (Lin et al., 2019). It is likely that correlations between relative SLR and TC precipitation and ETC activity may well impact future flood hazard in some regions.

5. Conclusion

The results of this analysis indicate that relative SLR is correlated with aspects of TC activity over much of the western North Atlantic and North West Pacific, suggesting that progressive warming will compound future flood hazard in these regions. Increases in PI, coupled with more favorable vertical wind shear also suggest a large scale environment more conducive to TCs in these regions. Based on analyses of synthetic TCs and hydrodynamic modeling, we find that large scale co-variability impacts local flood hazard, particularly at New Orleans, Wilmington and Charleston, with future storm tides predicted to increase with warming due to relative SLR coupled with progressively stronger and slower moving TCs along the US East Coast, even if TC frequency remain unchanged.

We have found that by focusing on a subset of AOGCMs that do not reflect the full distribution of GSAT changes within the emission scenario, and by assuming independence between SLR and storm tide change, coastal flood hazard assessments may not accurately capture future coastal flood hazard. By neglecting correlated changes at Wilmington NC, as an example, the average of projected change to the historical 100-year flood level is under-estimated by 12%. We recommend that future studies that focus on a specific emissions scenario: (a) construct SLR and TC projections inherent to each model to ensure that correlations are incorporated, (b) consider extremes as well as average projections, given that model variation is strongly modulated by joint variability related to GSAT and (c) be mindful of the GSAT change and ECS of each CMIP6 model used, as selection bias may substantially alter flood hazard projections.

Our paper is novel in that we explore global scale correlations between TC activity and relative SLR that includes contributions from land ice loss and associated GRD fingerprints and from non-climatic changes. We also conduct climatological-hydrodynamic modeling to quantify the impact of correlations on future flood hazard and explore correlations between SLR and synthetic TCs. We show that aspects of TC activity change are likely to co-vary with relative SLR, meaning that flood hazard assessments that neglect the joint influence of these factors may misrepresent future flood hazard. We recommend that future studies on coastal flood hazards explore correlated changes between future TCs, ETCs, precipitation and relative SLR.

Data Availability Statement

CMIP6 data is available from https://esgf-node.llnl.gov/projects/cmip6/. Output from ADCIRC modeling is available from the authors upon reasonable request. Code used in this analysis can be obtained at https://github.com/JWLockwood/LOCKWOOD2022.

Acknowledgments
We are grateful to D. J Rasmussen who provided helpful comments on the manuscript. The authors thank T. Frederikse for providing output from the GRD model. J. W. Lockwood was supported by the Princeton University Fellowship in Natural Sciences and Engineering. R. E. Kopp was supported by NSF award ICER-1663807, NASA award 80NSSC20K1724, and NASA JPL project 105393.509496.02.08.13.31. R. E. Kopp, N. Lin, and M. Oppenheimer were supported by the National Science Foundation (NSF) as part of the Megalopolitan Coastal Transformation Hub (MACH) under NSF award ICER-2103754. N. Lin was supported by NSF award 1652448. This publication was supported by the Princeton University Library Open Access Fund.

References

Argus, D., Peltier, W., Drummond, R., & Moore, A. (2014). The Antarctica component of postglacial rebound model ICE-6G_C (VM5a) based on GPS positioning, exposure age dating of ice thicknesses, and relative sea level histories. *Geophysical Journal International*, *198*, 537–563. https://doi.org/10.1093/gji/ggu140

Bamber, J. L., Oppenheimer, M., Kopp, R. E., Aspinall, W. P., & Cooke, R. M. (2019). Ice sheet contributions to future sea-level rise from structured expert judgment. *Proceedings of the National Academy of Sciences*, *116*(23), 11195–11200. https://doi.org/10.1073/pnas.1817205116

Bhatia, K., Vecchi, G., Murakami, H., Underwood, S., & Kossin, J. (2018). Projected response of tropical cyclone intensity and intensification in a global climate model. *Journal of Climate*, *31*(20), 8281–8303. https://doi.org/10.1175/JCLI-D-17-0898.1

Bilskie, M., Angel, D., Yoskowitz, D., & Hagen, S. (2020). *Future flood risk exacerbated by the dynamic impacts of sea level rise*. https://doi.org/10.21203/rs.3.rs-63173/v1

Bilskie, M., Hagen, S., Alizad, K., Medeiros, S., Passeri, D., Needham, H., & Cox, A. (2016). Dynamic simulation and numerical analysis of hurricane storm surge under sea level rise with geomorphologic changes along the northern Gulf of Mexico. *Earth's Future*, *4*, 177–193. https://doi.org/10.1002/2015EF000347

Bilskie, M., Hagen, S. C., Medeiros, S. C., & Passeri, D. L. (2014). Dynamics of sea level rise and coastal flooding on a changing landscape. *Geophysical Research Letters*, *41*(3), 927–934. https://doi.org/10.1002/2013gl058759

Bister, M., & Emanuel, K. A. (1998). Dissipative heating and hurricane intensity. *Meteorology and Atmospheric Physics*, *65*(3–4), 233–240. https://doi.org/10.1007/BF01030791

Booth, J., Rieder, H., & Kushnir, Y. (2016). Comparing hurricane and extratropical storm surge for the Mid-Atlantic and Northeast Coast of the United States for 1979–2013. *Environmental Research Letters*, *11*, 094004. https://doi.org/10.1088/1748-9326/11/9/094004

Brunner, L., Pendergrass, A. G., Lehner, F., Merrifield, A. L., Lorenz, R., & Knutti, R. (2020). Reduced global warming from CMIP6 projections when weighting models by performance and independence. *Earth System Dynamics*, *11*(4), 995–1012. https://doi.org/10.5194/esd-11-995-2020

Buchanan, M., Kopp, R., Oppenheimer, M., & Tebaldi, C. (2016). Allowances for evolving coastal flood risk under uncertain local sea-level rise. *Climatic Change*, *137*(3–4), 347–362. https://doi.org/10.1007/s10584-016-1664-7

Camargo, S. J. (2013). Global and regional aspects of tropical cyclone activity in the CMIP5 models. *Journal of Climate*, *26*(24), 9880–9902. https://doi.org/10.1175/JCLI-D-12-00549.1

Camargo, S. J., & Wing, A. A. (2021). Increased tropical cyclone risk to coasts. *Science*, *371*(6528), 458–459. https://doi.org/10.1126/science.abg3651

Chan, J. C. (2005). The physics of tropical cyclone motion. *Annual Review of Fluid Mechanics*, *37*(1), 99–128. https://doi.org/10.1146/annurev.fluid.37.061903.175702

Chavas, D. R., Lin, N., & Emanuel, K. (2015). A model for the complete radial structure of the tropical cyclone wind field. Part I: Comparison with observed structure. *Journal of the Atmospheric Sciences*, *72*(9), 3647–3662. https://doi.org/10.1175/jas-d-15-0014.1

Chavas, D. R., Lin, N., & Emanuel, K. (2016). A model for the complete radial structure of the tropical cyclone wind field. Part II: Wind field variability. *Journal of the Atmospheric Sciences*, *72*(9), 3093–3113. https://doi.org/10.1175/JAS-D-15-0185.1

Church, J., Clark, P., Cazenave, A., Gregory, J., Jevrejeva, S., Levermann, A., et al. (2013). Climate change 2013: The physical science basis. contribution of working group I to the fifth assessment report of the intergovernmental panel on climate change. *Sea Level Change*, 1138–1191.

Coles, S. (2001). *An introduction to statistical modeling of extreme values*.

Deconto, R. M., Pollard, D., Alley, R. B., Velicogna, I., Gasson, E., Gomez, N., et al. (2021). The Paris Climate Agreement and future sea-level rise from Antarctica. *Nature*, *593*. https://doi.org/10.1038/s41586-021-03427-0

De Dominicis, M., Wolf, J., Jevrejeva, S., Zheng, P., & Hu, Z. (2020). Future interactions between sea level rise, tides, and storm surges in the world's largest urban area. *Geophysical Research Letters*, *47*(4). https://doi.org/10.1029/2020GL087002

Emanuel, K. (2021). Response of global tropical cyclone activity to increasing CO_2: Results from downscaling CMIP6 models. *Journal of Climate*, *34*, 57–70. https://doi.org/10.1175/jcli-d-20-0367.1

Emanuel, K., & Nolan, D. S. (2004). Tropical cyclone activity and the global climate system. *26th Conference on Hurricanes and Tropical Meteorology*, 240–241.

Emanuel, K., Sundararajan, R., & Williams, J. (2008). Hurricanes and global warming: Results from downscaling IPCC AR4 simulations. *Bulletin of the American Meteorological Society*, *89*(3), 347–368. https://doi.org/10.1175/BAMS-89-3-347

Emanuel, K. A. (2004). *Tropical cyclone energetics and structure*.

Emanuel, K. A. (2013). Downscaling CMIP5 climate models shows increased tropical cyclone activity over the 21st century. *Proceedings of the National Academy of Sciences of the United States of America*, *110*(30), 12219–12224. https://doi.org/10.1073/pnas.1301293110

Eyring, V., Bony, S., Meehl, G. A., Senior, C. A., Stevens, B., Stouffer, R. J., & Taylor, K. E. (2016). Overview of the Coupled Model Intercomparison Project Phase 6 (CMIP6) experimental design and organization. *Geoscientific Model Development*, *9*(5), 1937–1958. https://doi.org/10.5194/gmd-9-1937-2016

Farinotti, D., Huss, M., Fürst, J., Landmann, J., Machguth, H., Maussion, F., & Pandit, A. (2019). A consensus estimate for the ice thickness distribution of all glaciers on Earth. *Nature Geoscience*, *12*. https://doi.org/10.1038/s41561-019-0300-3

Fox-Kemper, B., Hewitt, H. T., Xiao, C., Aalgeirsdóttir, G., Drijfhout, S. S., Edwards, T. L., et al. (2021). Ocean, cryosphere and sea level change. In *Climate change 2021: The physical science basis. Contribution of working group I to the sixth assessment report of the intergovernmental panel on climate change*. Cambridge University Press.

Frederikse, T., Buchanan, M. K., Lambert, E., Kopp, R. E., Oppenheimer, M., Rasmussen, D. J., & de Wal, R. S. (2020). Antarctic Ice Sheet and emission scenario controls on 21st-century extreme sea-level changes. *Nature Communications*, *11*(1), 1–11. https://doi.org/10.1038/s41467-019-14049-6

Fürst, J. J., Goelzer, H., & Huybrechts, P. (2015). Ice-dynamic projections of the Greenland ice sheet in response to atmospheric and oceanic warming. *The Cryosphere*, *9*(3), 1039–1062. https://doi.org/10.5194/tc-9-1039-2015

Garner, A. J., Kopp, R., & Horton, B. (2021). *Evolving tropical cyclone tracks in the North Atlantic in a warming climate*. https://doi.org/10.1130/abs/2021AM-363502

Garner, A. J., Mann, M. E., Emanuel, K. A., Kopp, R. E., Lin, N., Alley, R. B., et al. (2017). Impact of climate change on New York City's coastal flood hazard: Increasing flood heights from the preindustrial to 2300 CE. *Proceedings of the National Academy of Sciences*, *114*(45), 11861–11866. https://doi.org/10.1073/pnas.1703568114

Genthon, C., Krinner, G., & Castebrunet, H. (2009). Antarctic precipitation and climate-change predictions: Horizontal resolution and margin vs plateau issues. *Annals of Glaciology*, *50*(50), 55–60. https://doi.org/10.3189/172756409787769681

Gori, A., Lin, N., Xi, D., & Emanuel, K. (2022). Tropical cyclone climatology change greatly exacerbates us joint rainfall-surge hazard. *Nature Climate Change*. Retrieved from https://assets.researchsquare.com/files/rs-805581/v1_covered.pdf?c=1631876900

Gregory, M. J., Griffies, S. M., Hughes, C. W., Lowe, J. A., Church, J. A., Fukimori, I., et al. (2019). Concepts and terminology for sea level : Mean , variability and change both local and global. *Surveys in Geophysics*, 0123456789. https://doi.org/10.1007/s10712-019-09525-z

Gregory, M. J., & Huybrechts, P. (2006). Ice-sheet contributions to future sea-level change. *Philosophical Transactions of the Royal Society A: Mathematical, Physical & Engineering Sciences*, *364*(1844), 1709–1732. https://doi.org/10.1098/rsta.2006.1796

Griffies, S. M., Danabasoglu, G., Durack, P. J., Adcroft, A. J., Balaji, V., Böning, C. W., et al. (2016). OMIP contribution to CMIP6: Experimental and diagnostic protocol for the physical component of the Ocean Model Intercomparison Project. *Geoscientific Model Development*, *9*(9), 3231–3296. https://doi.org/10.5194/gmd-9-3231-2016

Griffies, S. M., & Greatbatch, R. J. (2012). Physical processes that impact the evolution of global mean sea level in ocean climate models. *Ocean Modelling*, *51*, 37–72. https://doi.org/10.1016/j.ocemod.2012.04.003

Griffies, S. M., Yin, J., Durack, P. J., Goddard, P., Bates, S. C., Behrens, E., et al. (2014). An assessment of global and regional sea level for years 1993–2007 in a suite of interannual CORE-II simulations. *Ocean Modelling*, *78*, 35–89. https://doi.org/10.1016/j.ocemod.2014.03.004

Hausfather, Z., & Peters, G. P. (2020). Heading in here running to two lines. *Nature*.

Hermans, T. H. J., Gregory, J. M., Palmer, M. D., Ringer, M. A., Katsman, C. A., & Slangen, A. B. A. (2021). Projecting global mean sea-level change using CMIP6 models. *Geophysical Research Letters*, *48*(5), e2020GL092064. https://doi.org/10.1029/2020gl092064

Hock, R., Bliss, A., Marzeion, B., Giesen, R. H., Hirabayashi, Y., Huss, M., et al. (2019). GlacierMIP—A model intercomparison of global-scale glacier mass-balance models and projections. *Journal of Glaciology*, *65*(251), 453–467. https://doi.org/10.1017/jog.2019.22

Hunter, J. (2011). A simple technique for estimating an allowance for uncertain sea-level rise. *Climatic Change*, *113*. https://doi.org/10.1007/s10584-011-0332-1

Idier, D., Bertin, X., Thompson, P., & Pickering, M. D. (2019). Interactions between mean sea level, tide, surge, waves and flooding: Mechanisms and contributions to sea level variations at the coast. *Surveys in Geophysics*, *40*(6), 1603–1630. https://doi.org/10.1007/s10712-019-09549-5

Kang, S. M., & Lu, J. (2012). Expansion of the Hadley cell under global warming: Winter versus summer. *Journal of Climate*, *25*(24), 8387–8393. https://doi.org/10.1175/jcli-d-12-00323.1

Kirezci, E., Young, I., Ranasinghe, R., Muis, S., Nicholls, R., Lincke, D., & Hinkel, J. (2020). Projections of global-scale extreme sea levels and resulting episodic coastal flooding over the 21st century. *Scientific Reports*, *10*, 11629. https://doi.org/10.1038/s41598-020-67736-6

Kittel, C., Amory, C., Agosta, C., Jourdain, N. C., Hofer, S., Delhasse, A., et al. (2021). Diverging future surface mass balance between the Antarctic ice shelves and grounded ice sheet. *The Cryosphere*, (pp. 1215–1236). https://doi.org/10.5194/tc-15-1215-2021

Knutson, T., Camargo, S. J., Chan, J. C. L., Emanuel, K., Ho, C.-H., Kossin, J., et al. (2020). Tropical cyclones and climate change assessment: Part II: Projected response to anthropogenic warming. *Bulletin of the American Meteorological Society*, *101*(3), E303–E322. https://doi.org/10.1175/BAMS-D-18-0194.1

Knutson, T. R., Sirutis, J., Zhao, M., Tuleya, R., Bender, M., Vecchi, G., et al. (2015). Global projections of intense tropical cyclone activity for the late twenty-first century from dynamical downscaling of CMIP5/RCP4.5 scenarios. *Journal of Climate*, *28*, 7203–7224. https://doi.org/10.1175/jcli-d-15-0129.1

Kopp, R. E., Deconto, R. M., Bader, D. A., Hay, C. C., Radley, M., Kulp, S., et al. (2017). Earth's future evolving understanding of Antarctic ice-sheet physics and ambiguity in probabilistic sea-level projections. *Earth's Future*, *5*(12), 1217–1233.

Kopp, R. E., Hay, C. C., Little, C. M., & Mitrovica, J. X. (2015). Geographic variability of sea-level change. *Current Climate Change Reports*, *1*(3), 192–204. https://doi.org/10.1007/s40641-015-0015-5

Kopp, R. E., Horton, R. M., Little, C. M., Mitrovica, J. X., Oppenheimer, M., Rasmussen, D. J., et al. (2014). Earth's Future Probabilistic 21st and 22nd century sea-level projections at a global network of tide-gauge sites. *Earth ' s Future*, *2*(8)(pp. 383–407). https://doi.org/10.1002/2014EF000239

Kossin, J. P. (2018). A global slowdown of tropical-cyclone translation speed. *Nature*, *558*(7708), 104–107. https://doi.org/10.1038/s41586-018-0158-3

Lambert, E., Le Bars, D., Goelzer, H., & van de Wal, R. S. (2021). Correlations between sea-level components are driven by regional climate change. *Earth's Future*, *9*(2), e2020EF001825. https://doi.org/10.1029/2020ef001825

Levermann, A., Winkelmann, R., Albrecht, T., Goelzer, H., Golledge, N. R., Greve, R., et al. (2020). Projecting Antarctica's contribution to future sea level rise from basal ice shelf melt using linear response functions of 16 ice sheet models (LARMIP-2). *Earth System Dynamics*, *11*(1), 35–76. https://doi.org/10.5194/esd-11-35-2020

Li, J., Sun, C., & Jin, F.-F. (2013). NAO implicated as a predictor of Northern Hemisphere mean temperature multidecadal variability. *Geophysical Research Letters*, *40*(20), 5497–5502. https://doi.org/10.1002/2013GL057877

Li, W., Li, L., Ting, M., & Liu, Y. (2012). Intensification of Northern Hemisphere near-surface subtropical highs in a warming climate. *Nature Geoscience*. https://doi.org/10.1038/ngeo1590

Lin, N., Emanuel, K., Oppenheimer, M., & Vanmarcke, E. (2012). Physically based assessment of hurricane surge threat under climate change. *Nature Climate Change*, *2*, 462–467. https://doi.org/10.1038/nclimate1389

Lin, N., Emanuel, K. A., Smith, J. A., & Vanmarcke, E. (2010). Risk assessment of hurricane storm surge for New York City. *Journal of Geophysical Research*, *115*(D18). https://doi.org/10.1029/2009JD013630

Lin, N., Kopp, R. E., Horton, B. P., & Donnelly, J. P. (2016). Hurricane Sandy's flood frequency increasing from year 1800 to 2100. *Proceedings of the National Academy of Sciences*, *113*(43), 12071–12075. https://doi.org/10.1073/pnas.1604386113

Lin, N., Marsooli, R., & Colle, B. (2019). Storm surge return levels induced by mid-to-late-twenty-first-century extratropical cyclones in the Northeastern United States. *Climatic Change*, *154*. https://doi.org/10.1007/s10584-019-02431-8

Little, C. M., Horton, R. M., Kopp, R. E., Oppenheimer, M., Vecchi, G. A., & Villarini, G. (2015). Joint projections of US East Coast sea level and storm surge. *Nature Climate Change*, *5*(12), 1114–1120. https://doi.org/10.1038/nclimate2801

Liu, Y., Asher, T. G., & Irish, J. L. (2019). Physical drivers of changes in probabilistic surge hazard under sea level rise. *Earth's Future*, *7*(7), 819–832. https://doi.org/10.1029/2019ef001216

Lu, J., Vecchi, G. A., & Reichler, T. (2007). Expansion of the Hadley cell under global warming. *Geophysical Research Letters*, *34*(6). https://doi.org/10.1029/2006gl028443

Luettich, R., Jr., Westerink, J., & Scheffner, N. (1992). ADCIRC: An advanced three-dimensional circulation model for shelves, coasts, and estuaries. Report 1. Theory and methodology of ADCIRC-2DDI and ADCIRC-3DL. *Dredging Research Program Technical Report DRP-92-6*, 143.

Marsooli, R., & Lin, N. (2020). Impacts of climate change on hurricane flood hazards in Jamaica Bay, New York. *Climatic Change*, *163*, 1–19. https://doi.org/10.1007/s10584-020-02932-x

Marsooli, R., Lin, N., Emanuel, K., & Feng, K. (2019). Climate change exacerbates hurricane flood hazards along US Atlantic and Gulf Coasts in spatially varying patterns. *Nature Communications*, *10*(1), 1–9. https://doi.org/10.1038/s41467-019-11755-z

Marzeion, B., Hock, R., Anderson, B., Bliss, A., Champollion, N., Fujita, K., et al. (2020). Partitioning the uncertainty of ensemble projections of global glacier mass change. *Earth's Future*, *8*(7), e2019EF001470. https://doi.org/10.1029/2019ef001470

Merrill, R. T. (1988). Environmental influences on hurricane intensification. *Journal of the Atmospheric Sciences*, *45*(11), 1678–1687. https://doi.org/10.1175/1520-0469(1988)045<1678:eiohi>2.0.co;2

Oppenheimer, M., Glavovic, B., Hinkel, J., van de Wal, R., Magnan, A. K., Abd-Elgawad, A., et al. (2019). Sea level rise and implications for low lying islands, coasts and communities. *IPCC Special Report on the Ocean and Cryosphere in a Changing Climate*, *355*(6321), 126–129.

Peltier, W. R., Argus, D. F., & Drummond, R. (2015). Space geodesy constrains ice age terminal deglaciation: The global ICE-6G_C (VM5a) model. *Journal of Geophysical Research: Solid Earth*, *120*(1), 450–487. https://doi.org/10.1002/2014jb011176

Perrette, M., Landerer, F., Riva, R., Frieler, K., & Meinshausen, M. (2013). A scaling approach to project regional sea level rise and its uncertainties. *Earth System Dynamics*, *4*(1), 11–29. https://doi.org/10.5194/esd-4-11-2013

Rasmussen, D. J., Bittermann, K., Buchanan, M. K., Kulp, S., Strauss, B. H., Kopp, R. E., & Oppenheimer, M. (2018). Extreme sea level implications of 1.5°c, 2.0°c, and 2.5°c temperature stabilization targets in the 21st and 22nd centuries. *Environmental Research Letters*, *13*(3), 034040. https://doi.org/10.1088/1748-9326/aaac87

Reed, A. J., Mann, M. E., Emanuel, K. A., Lin, N., Horton, B. P., Kemp, A. C., & Donnelly, J. P. (2015). Increased threat of tropical cyclones and coastal flooding to New York City during the anthropogenic era. *Proceedings of the National Academy of Sciences*, *112*(41), 12610–12615. https://doi.org/10.1073/pnas.1513127112

Resio, D. T., & Irish, J. L. (2015). *Tropical cyclone storm surge risk* (pp. 74–84). https://doi.org/10.1007/s40641-015-0011-9

Rios-Berrios, R., & Torn, R. D. (2017). Climatological analysis of tropical cyclone intensity changes under moderate vertical wind shear. *Monthly Weather Review*, *145*(5), 1717–1738. https://doi.org/10.1175/mwr-d-16-0350.1

Sobel, A. H., Camargo, S. J., Hall, T. M., Lee, C.-Y., Tippett, M. K., & Wing, A. A. (2016). Human influence on tropical cyclone intensity. *Science*, *353*(6296), 242–246. https://doi.org/10.1126/science.aaf6574

Strauss, B., Orton, P., Bittermann, K., Buchanan, M., Gilford, D., Kopp, R., et al. (2021). Economic damages from Hurricane Sandy attributable to sea level rise caused by anthropogenic climate change. *Nature Communications*, *12*(1). https://doi.org/10.1038/s41467-021-22838-1

Tamisiea, M. E., & Mitrovica, J. X. (2011). The moving boundaries of sea level change: Understanding the origins of geographic variability. *Oceanography*. https://doi.org/10.5670/oceanog.2011.25

Tang, B., & Camargo, S. J. (2014). Environmental control of tropical cyclones in CMIP5: A ventilation perspective. *Journal of Advances in Modeling Earth Systems*, *6*(1), 115–128. https://doi.org/10.1002/2013ms000294

Tebaldi, C., Strauss, B. H., & Zervas, C. E. (2012). Modelling sea level rise impacts on storm surges along US coasts. *Environmental Research Letters*, *7*(1), 014032. https://doi.org/10.1088/1748-9326/7/1/014032

Ting, M., Kossin, J., Camargo, S., & Li, C. (2019). Past and future hurricane intensity change along the US East Coast. *Scientific Reports*, *9*. https://doi.org/10.1038/s41598-019-44252-w

Trenberth, K., Fasullo, J., & Shepherd, T. (2015). Attribution of climate extreme events. *Nature Climate Change*, *5*, 725–730. https://doi.org/10.1038/nclimate2657

Vecchi, G. A., Delworth, T. L., Murakami, H., Underwood, S. D., Wittenberg, A. T., Zeng, F., et al. (2019). Tropical cyclone sensitivities to CO2 doubling: Roles of atmospheric resolution, synoptic variability and background climate changes. *Climate Dynamics*, *53*(9) 10. https://doi.org/10.1007/s00382-019-04913-y

Vecchi, G. A., & Soden, B. J. (2007a). Effect of remote sea surface temperature change on tropical cyclone potential intensity. *Nature*, *450*, 1066–1070. https://doi.org/10.1038/nature06423

Vecchi, G. A., & Soden, B. J. (2007b). Global warming and the weakening of the tropical circulation. *Journal of Climate*, *20*(17), 4316–4340. https://doi.org/10.1175/jcli4258.1

Vecchi, G. A., & Soden, B. J. (2007c). Increased tropical Atlantic wind shear in model projections of global warming. *Geophysical Research Letters*, *34*(8), 1–5. https://doi.org/10.1029/2006GL028905

Villarini, G., & Vecchi, G. A. (2013). Projected increases in North Atlantic tropical cyclone intensity from CMIP5 models. *Journal of Climate*, *26*(10), 3231–3240. https://doi.org/10.1175/JCLI-D-12-00441.1

Vousdoukas, M., Mentaschi, L., Voukouvalas, E., Verlaan, M., Jevrejeva, S., Jackson, L., & Feyen, L. (2018). Global probabilistic projections of extreme sea levels show intensification of coastal flood hazard. *Nature Communications*, *9*. https://doi.org/10.1038/s41467-018-04692-w

Wahl, T., Jain, S., Bender, J., Meyers, S. D., & Luther, M. E. (2015). Increasing risk of compound flooding from storm surge and rainfall for major US cities. *Nature Climate Change*, *5*(12), 1093–1097. https://doi.org/10.1038/nclimate2736

Wang, C., Soden, B. J., Yang, W., & Vecchi, G. A. (2021). Compensation between cloud feedback and aerosol-cloud interaction in CMIP6 models. *Geophysical Research Letters*, *48*(4), e2020GL091024. https://doi.org/10.1029/2020gl091024

Wang, S., & Toumi, R. (2021). Recent migration of tropical cyclones toward coasts. *Science*, *371*(6528), 514–517. https://doi.org/10.1126/science.abb9038

Westerink, J., Luettich, R., Jr., Blain, C., & Scheffner, N. (1994). *Adcirc: An advanced three-dimensional circulation model for shelves, coasts, and estuaries. report 2. user's manual for adcirc-2ddi*. Army Engineer Waterways Experiment Station Vicksburg Ms, 168.

Woodruff, J. D., Irish, J. L., & Camargo, S. J. (2013). Coastal flooding by tropical cyclones and sea-level rise. *Nature*, *504*(7478), 44–52. https://doi.org/10.1038/nature12855

Yamada, Y., Oouchi, K., Satoh, M., Tomita, H., & Yanase, W. (2010). Projection of changes in tropical cyclone activity and cloud height due to greenhouse warming: Global cloud-system-resolving approach. *Geophysical Research Letters*, *37*(7), 1–5. https://doi.org/10.1029/2010GL042518

Yin, J., Griffies, S. M., Winton, M., Zhao, M., & Zanna, L. (2020). Response of storm-related extreme sea level along the U.S. Atlantic coast to combined weather and climate forcing. *Journal of Climate*, *33*(9), 3745–3769. https://doi.org/10.1175/JCLI-D-19-0551.1

Zscheischler, J., & Seneviratne, S. I. (2017). Dependence of drivers affects risks associated with compound events. *Science Advances*, *3*(6), 1–11. https://doi.org/10.1126/sciadv.1700263

Zscheischler, J., Westra, S., van den Hurk, B. J. J. M., Seneviratne, S. I., Ward, P. J., Pitman, A., et al. (2018). Future climate risk from compound events. *Nature Climate Change*, *8*(6), 469–477. https://doi.org/10.1038/s41558-018-0156-3